



Enabling efficient heat-to-electricity generation at the mesoscale†

Cite this: DOI: 10.1039/c7ee00366h

Walker R. Chan,^{id}*^a Veronika Stelmakh,^{id}^{ab} Michael Ghebrebrhan,^c Marin Soljačić,^d John D. Joannopoulos^{ad} and Ivan Čelanović^a

Received 7th February 2017,
Accepted 9th May 2017

DOI: 10.1039/c7ee00366h

rsc.li/ees

We present a technology that efficiently harnesses the energy content of hydrocarbon fuels in a volume that is only a fraction of a cubic inch. A propane-fueled microcombustor heats a photonic crystal emitter to incandescence and the resulting spectrally-confined thermal radiation drives low-bandgap PV cells to generate electricity. We overcome the technical challenges that are currently limiting thermophotovoltaics in the following ways: we develop new fabrication processes; we adopt high-temperature alloys to improve the thermo-mechanical stability; we adopt commercial polycrystalline tantalum to fabricate large-area photonic crystals; and finally, we develop a passivation coating for improved thermo-chemical stability. We demonstrate unprecedented heat-to-electricity efficiencies exceeding 4%, greater than the 2–3% efficiencies that were previously thought to be the practical limit, and we predict that over 12% efficiency is achievable with only engineering optimization. For reference, a 1.5% efficiency corresponds to the energy density of lithium ion batteries. This work opens new opportunities to free portable electronics, robots, and small drones from the constraints of bulky power sources.

Introduction

In this paper, we present a technology that generates watts of electricity from a heat input that is similar to that of a lighter, in a volume that is only a fraction of a cubic inch. We attain unprecedented efficiencies, exceeding 4% in a mesoscale form factor, where previous heat-to-electricity system efficiencies of 2–3% were thought to be the practical limit.^{1–4} Moreover, we show computationally that a 12.6% efficiency should be achievable with only engineering optimization and no further

Broader context

At small scales (<100 W), batteries are the only currently available energy source and are already close to their theoretical limit; in contrast, hydrocarbon fuels have 60 times the energy density (a 1.5% fuel-to-electricity conversion efficiency corresponds to the energy density of lithium ion batteries). Thus, harnessing the energy content of hydrocarbon fuels on the mesoscale should pave the way to transformative increases in portable power generation. Mesoscale generators aim to fill the gap between batteries and conventional mechanical generators, where energy demand is burgeoning. Mesoscale fuel-to-electricity conversion is challenging because the vastly different length scales compared to those of conventional generators result in different geometric scaling and different phenomenological behaviors. Micro-mechanical heat engines, fuel cells, thermoelectrics, and thermophotovoltaics are actively being applied.

scientific breakthroughs. In our system, a propane-fueled microcombustor heats a photonic crystal emitter to incandescence and the resulting tailored thermal radiation drives low-bandgap photovoltaic (PV) cells to generate electricity. We overcome current bottlenecks by employing new high-temperature material systems, processing, and fabrication techniques, accomplishing record efficiencies in the heat-to-electricity conversion. At these small scales, batteries are the only currently available energy source and they are already close to their theoretical limit.⁵ In contrast, hydrocarbon fuels have 60 times the energy density of batteries (a 1.5% fuel-to-electricity conversion efficiency corresponds to the energy density of lithium ion batteries), and therefore they promise order-of-magnitude increases in their energy storage and conversion. Thus, harnessing the energy content of hydrocarbon fuels on the mesoscale should pave the way for transformative increases in portable power generation. Mesoscale generators aim to fill the gap between batteries and conventional mechanical generators, where energy demand is burgeoning.

Unconventional and fundamentally different energy conversion methods are required at the mesoscale because the vastly different length scales compared to those of conventional generators result in different geometric scaling (*e.g.*, surface area to volume ratio) and different phenomenological behaviors

^a Institute for Soldier Nanotechnologies, Massachusetts Institute of Technology, 77 Massachusetts Avenue, Cambridge, MA 02139, USA. E-mail: wrchan@mit.edu

^b Department of Electrical Engineering, Massachusetts Institute of Technology, 77 Massachusetts Avenue, Cambridge, MA 02139, USA

^c U.S. Army Natick Soldier Research, Development, and Engineering Center, 1 4th Ave., Natick, MA 01760, USA

^d Department of Physics, Massachusetts Institute of Technology, 77 Massachusetts Avenue, Cambridge, MA 02139, USA

† Electronic supplementary information (ESI) available. See DOI: 10.1039/c7ee00366h

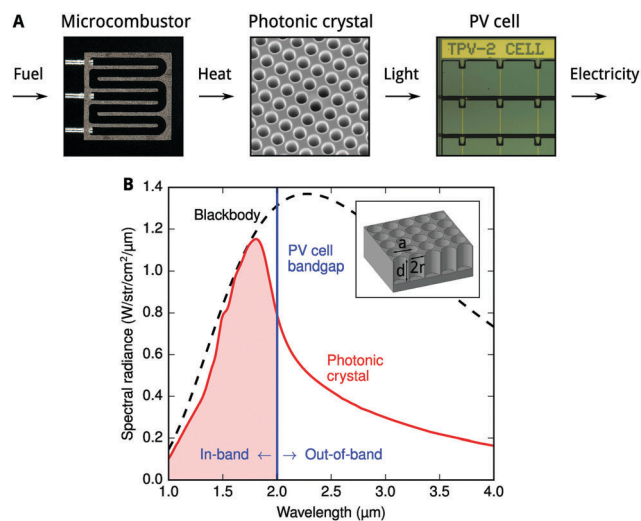


Fig. 1 (A) In the TPV energy conversion process, fuel and oxygen react in a microcombustor to generate heat, which brings a photonic crystal emitter to incandescence. The resulting spectrally-confined thermal radiation drives a low bandgap PV cell to generate electricity. (B) Simulated spectral radiance at 1000 °C normal to the surface of the photonic crystal and a blackbody are plotted. The photonic crystal's emission spectrum is engineered to primarily fall below the bandgap of the PV cell, and this in-band radiation, highlighted in red, is converted to electricity. Inset: The photonic crystal is composed of a square array of cylindrical cavities, and its cutoff wavelength can be tuned by varying the radius, r , period, a , and depth, d .

(*e.g.*, laminar and turbulent flow). Micro-mechanical heat engines,^{6,7} fuel cells,^{8,9} and thermoelectrics^{3,4} are actively being applied. Indeed, solid oxide fuel cells have demonstrated efficiencies of 45–60% in 10–220 kW_e systems,¹⁰ but face numerous challenges in their miniaturization including thermal and mechanical stability, fuel utilization, and the auxiliary and support systems. In our research, we chose to work within the heat-to-electricity framework of thermophotovoltaic (TPV) energy conversion, as shown in Fig. 1A. Our choice was dictated by the following points: TPV devices have no moving parts and thus do not suffer from increased frictional losses arising from miniaturization; the high-temperature continuous combustion process enables TPV devices to efficiently process fuel at the mesoscale and be more readily adapted to chemically impure fuel sources such as biofuels; and the physical separation of the thermal and electrical circuits greatly simplifies engineering efforts. Previous work introduced the basic principles for potential improvements in TPV devices² that included the key components: a microcombustor,¹¹ a photonic crystal,^{12–16} and PV cells.^{17–19} Nevertheless, several fundamental challenges severely limited the feasibility of a practical system. These challenges include the high-temperature thermo-mechanical stability arising from heterogeneous material systems; the integration of the microcombustor and photonic crystal emitter as well as the limited optical performance of those emitters that are capable of being integrated; the high-temperature thermo-chemical stability of refractory metals; and a lack of large-area wafer-quality refractory metal substrates. This work overcomes these challenges.

Specifically, we develop fabrication processes to integrate the microcombustor and photonic crystal; we adopt high-temperature alloys for the dramatically improved thermo-mechanical stability of the microcombustor; we adopt commercial polycrystalline tantalum to fabricate large-area wafer-quality substrates for the high-temperature photonic crystal; and finally, we develop a passivation coating for the improved high-temperature thermo-chemical stability of the photonic crystal materials.

Experimental

With the advances in photonic crystals and metamaterials coinciding with the advances in low-bandgap III–V PV cells, a high efficiency is possible because a large overlap of emission and absorption spectra occurs at readily achievable temperatures of 1000–1200 °C, as shown in Fig. 1B. Photonic crystals offer near blackbody emission resulting from cavity resonances at the desired wavelengths and near zero emission elsewhere due to the low loss of the substrate materials. Their emission spectra are primarily determined by their geometry rather than by their specific material properties, allowing the cutoff wavelength to be tuned to match the bandgap of the PV cell. Our 2D photonic crystal, which is composed of a square array of cylindrical cavities, as shown in the inset of Fig. 1B, addresses the challenges of large-area fabrication and integration, good optical performance, and high-temperature stability.²⁰ In this work, polycrystalline tantalum was used for its machinability, its fast etch rate and good etch selectivity, and the availability of high purity and high metallurgical quality substrates. Our simple fabrication method of interference lithography and deep reactive ion etching enables a uniform, large area (50 mm in diameter) to be reliably patterned. To integrate the photonic crystal with the microcombustor, we adopted the industrial process of diffusion brazing. The full fabrication process, including the substrate preparation and microcombustor integration, is described in the ESI.† Our photonic crystal is resistant to physical degradation because of its simple geometry, with a large radius of curvature, and the refractory metal substrate, with a high melting point and low vapor pressure, limiting atomic mobility. Additionally, it is resistant to chemical degradation, such as tantalum carbide formation, because of a conformal hafnium dioxide passivation layer. We have annealed samples for over 100 hours at 900 °C with no degradation in their structure or optical performance.

The experimental demonstration of the integrated TPV system required the design and fabrication of a microcombustor (described in the ESI†) as well as the experimental apparatus shown in Fig. 2A and B. For these experiments, we used pure oxygen in the combustion reaction to emulate exhaust recuperation, which is required in a portable, air-breathing system. Propane and oxygen entered the microcombustor through the inlet tubes, flowed through an internal serpentine channel where they reacted on the catalyst-coated walls (5% platinum on porous alumina), and exited through the outlet tube.¹¹ Heat was conducted through the channel walls to the photonic crystal emitters bonded to the top and bottom surfaces of the microcombustor, as shown

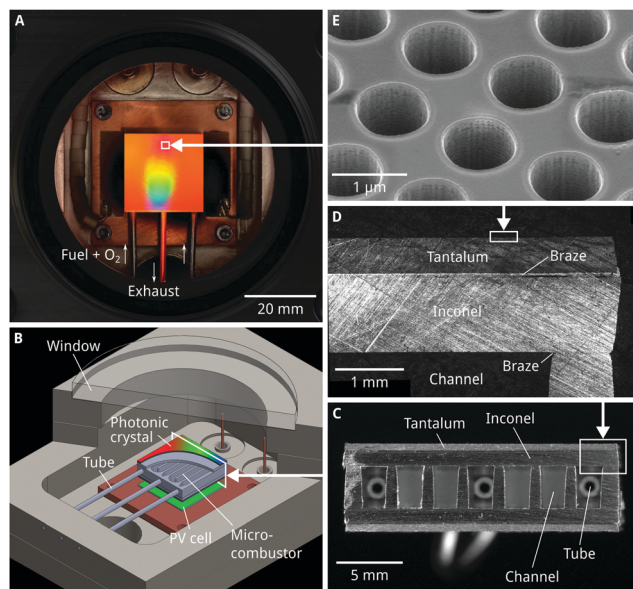


Fig. 2 (A) A photograph of the experimental setup during operation, where a diffraction pattern is visible on the photonic crystal from the ambient light. (B) A cutaway drawing of the experimental setup with labeled components. (C) A cross section of the microcombustor with unstructured tantalum substituted for the photonic crystal. (D) An optical micrograph of the corner of the Inconel microcombustor, with the diffusion brazed joint between the Inconel and tantalum visible. (E) A scanning electron micrograph of the surface of the photonic crystal.

in Fig. 2C and D. The photonic crystal emitted spectrally-confined thermal radiation that matched that of the InGaAs cells ($E_g = 2.0 \mu\text{m}$) mounted below the assembly.¹⁹ The experiment was housed in a custom vacuum chamber to suppress convection and prevent the degradation of the photonic crystal by reaction with air. A window was used in place of the top set of cells.

To ignite it, the microcombustor was heated to approximately 400°C with a halogen lamp through the window. Above that temperature, the propane kinetics over the catalyst were sufficient for autothermal operation, and the halogen lamp was shut off. Propane flows, corresponding to a total latent heat input of 20–100 W, were increased in small increments while maintaining an oxygen flow of 7.5 times that of propane (in an equivalence ratio of $\phi = 1.5$), and the steady-state electrical output at the maximum power point was measured. We characterized both a microcombustor with and without a photonic crystal emitter. For the microcombustor without the photonic crystal, the bare Inconel surface was oxidized by air until it was visibly black (emissivity of $\varepsilon \approx 0.8$) and it was then used as the emitter. The electrical measurements are shown in Fig. 3B, which is scaled for a full set of cells. We measured a 4.3% fuel-to-electricity conversion efficiency with the photonic crystal emitter and 1.5% with the oxidized Inconel emitter, for a fuel input of 100 W.

Discussion

We modeled the microcombustor with a custom heat transfer code incorporating the radiation from the front and back

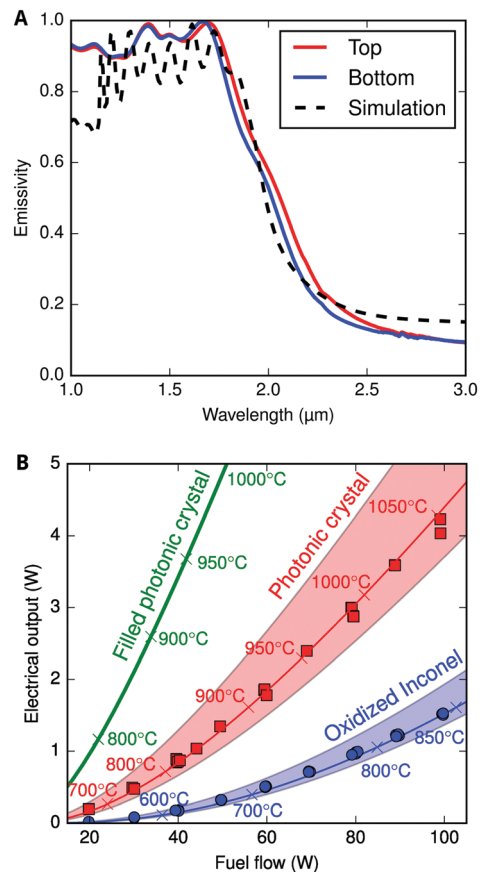


Fig. 3 (A) Measured and simulated at room temperature, the normal incidence emissivity of the photonic crystal. (B) The measured and simulated electrical power output as a function of fuel flow. The points are the experimental results. The lines and shaded bands are the simulation results, with the bands indicating a range of uncertain parameters. The simulated temperatures are indicated. Note that the filled photonic crystal (green line) has an electrical power output of 12.6 W at 100 W of fuel flow (not shown).

emitters and the edges of the microcombustor, the conduction through the support tubes, and the heat carried out by the hot exhaust gases. The hemispherically-averaged emissivity for the photonic crystal structure was computed using the Fourier modal method, a freely available software package,²¹ in which the optical dispersion was captured with a Lorentz–Drude model fitted to unstructured tantalum. The simulated and measured normal-incidence emissivities, plotted in Fig. 3A, agree well. Then, we used ray optics to accurately incorporate multiple scattering effects between the emitter and the PV cell, assuming purely diffuse emission and reflection.²² The PV cell was modeled using a single diode equivalent circuit methodology.²³ The microcombustor temperature, which is assumed to be uniform, was solved self-consistently. The simulated electrical power output and temperatures are shown in Fig. 3B; the shaded regions indicate the possible ranges of the experimental parameters, primarily the emissivity of the edges of the microcombustor.

We used the model to study the heat flows within the TPV systems with the photonic crystal and oxidized Inconel emitters, as shown in Table 1. Surprisingly, the in-band radiation increased

Table 1 The simulated systems with the oxidized Inconel emitter, photonic crystal emitter, and filled photonic crystal emitter. The hemispherically-averaged in-band and out-of-band emissivities of the emitters, edge emissivity, power distribution, efficiency, and temperature are listed

| Emitter | Oxidized Inconel | Photonic crystal | Filled photonic crystal |
|---|------------------|------------------|-------------------------|
| Emitter emissivity ($\epsilon_{in}/\epsilon_{out}$) | 0.80/0.80 | 0.58/0.18 | 0.92/0.16 |
| Edge emissivity | 0.80 | 0.55 | 0.15 |
| Fuel (W) | 100 | 100 | 100 |
| Exhaust (W) | 15.2 | 19.7 | 22.2 |
| Conduction (W) | 3.6 | 4.6 | 5.1 |
| Side radiation (W) | 27.3 | 32.8 | 12.5 |
| View factor loss (W) | 4.8 | 3.6 | 5.4 |
| Out-of-band radiation (W) | 46.9 | 24.5 | 15.2 |
| Cell inefficiencies (W) | 4.3 | 10.6 | 27.1 |
| Electricity (W) | 1.5 | 4.4 | 12.6 |
| Fuel-to-electricity efficiency (%) | 1.5 | 4.4 | 12.6 |
| Temperature ($^{\circ}\text{C}$) | 843 | 1054 | 1169 |

nearly three times in the case of the photonic crystal even though its hemispherically- and wavelength-averaged in-band emissivity was lower ($\epsilon = 0.59$ compared to $\epsilon = 0.8$). Because the photonic crystal suppressed the out-of-band radiation, the temperature increased by approximately 200°C , resulting in increased thermal radiation. From a practical point of view, the low out-of-band emissivity allows for a simpler system design without the need for photon recycling *via* a cold side filter placed between the emitter and PV cell,^{24–26} a difficult approach because of the wide range of angles and wavelengths that need to be filtered with high selectivity and low loss. Moreover, because of the photonic crystal's high in-band emissivity, electricity generation can compete favorably with other heat loss mechanisms and a readily achievable emitter temperature of 1000°C should provide greater than 500 mW cm^{-2} of cell area output. These factors are important in portable systems, as the low out-of-band emissivity minimizes the waste heat generated by the PV cell, and thus the heat sink size, and the high in-band emissivity minimizes the active area required for a specified electrical output as well as increasing efficiency.

Because the simulation identified two improvements that can reduce heat loss, we recognize that the efficiency can be improved beyond what was demonstrated experimentally in the photonic crystal system. Although an experimental demonstration of these improvements is beyond the scope of our present efforts, we can estimate their effects with our custom multi-physics simulation code. The first improvement is lower emissivity microcombustor edges. The edges are not only a significant portion of the total surface area but also radiate a disproportional amount when the photonic crystal suppresses the out-of-band radiation. If the emissivity of the edges can be decreased from the current value ($\epsilon = 0.55$) to that of polished tantalum ($\epsilon = 0.15$), a given temperature can be reached with a smaller fuel flow. We simulated this system using the same code but changed the value of the edge emissivity, predicting a fuel-to-electricity efficiency of 7.6% at 100 W of fuel input. The second improvement is the higher in-band emissivity of the photonic crystal, which can

proportionally decrease the heat loss from the microcombustor edges and other microcombustor heat loss mechanisms. Although at a normal incidence the photonic crystal has near blackbody in-band emissivity, the wavelength-averaged in-band emissivity is only $\epsilon = 0.59$ when averaged over all of the angles. By filling the cavities with a dielectric material, hafnium dioxide, we can increase the hemispherical in-band emissivity *via* several mechanisms: the physical and optical dimensions of the cavity are decoupled, allowing us to decrease the period and move the onset of diffraction well below the wavelength range of interest, even at oblique angles; and the optical density of states is increased and additional resonant peaks are created, further increasing the in-band emission. However, filling the cavities does slightly increase the out-of-band emissivity because the dielectric material increases the admittance of the cavities (approximated as waveguides) and hence the overall admittance of the effective medium (approximated as an area-weighted average between the flat surface and the cavity). Nevertheless, the simulations indicate that the resulting filled photonic crystal has omnidirectional thermal emission with an in-band emissivity of $\epsilon = 0.92$ while still having a low out-of-band emissivity of $\epsilon = 0.16$.²⁷ The higher in-band emissivity results in a larger electrical output for a given temperature. Again, we used the same simulation code, but with a filled-cavity photonic crystal in addition to low emissivity edges, to calculate the electrical output as a function of fuel flow, as shown in Fig. 3B, and the heat balance, as shown in Table 1. We predict a fuel-to-electricity efficiency of 12.6% at 100 W of fuel input, which is several times higher than that of the heat-to-electricity conversion methods that have been previously reported.

Conclusions

Such high energy density, multi-fuel powered, compact generators would free portable electronics, robots, and small drones from the constraints of bulky power sources. An even higher fuel-to-electricity efficiency is possible because there is room before the thermodynamic limit of TPV is reached.²⁸ One performance milestone can be achieved by improving the PV cell performance. State-of-the-art silicon solar PV cells operate at 85% of the Shockley–Queisser limit; on the other hand, state-of-the-art TPV cells only operate at $\sim 50\%$ of their thermodynamic limit because of non-radiative recombination mechanisms, series resistance, and non-ideal quantum efficiencies.²⁹ In other words, significant performance improvements are possible by following a similar research pathway, although low-bandgap semiconductors present a unique set of challenges compared to silicon. Another milestone can be achieved by improving the optical performance. Indeed, while the filled photonic crystal can achieve $\sim 70\%$ of the performance of an ideal (step function) emitter, as defined by the conversion of fuel to in-band radiation, a simple cold-side filter could improve this figure by further reducing the effective out-of-band emissivity near the cutoff. Further improvements may be possible, for example with a tandem PV-thermoelectric device³⁰ to recover the out-of-band radiation,

or with a thermoelectric device to recover the exhaust heat. Although technical challenges remain, this work demonstrates that a practical, portable TPV system is realizable in the near future.

Acknowledgements

The authors would like to thank C. Wang of the MIT Lincoln Laboratory for providing the InGaAs cells used in this work; B. Wilhite of Texas A&M University for performing the computation fluid dynamic simulations and assisting with the characterization of the microcombustor; J. Daley and T. Savas of MIT, and R. Geil of the University of North Carolina at Chapel Hill, for assistance with the fabrication of the photonic crystal; and M. Levine of MIT for a critical reading of the manuscript. The fabrication of the photonic crystal was done in part at NSL at MIT and at CNS at Harvard University, a member of the National Nanotechnology Infrastructure Network (NNIN), supported by the National Science Foundation (NSF) under NSF Award No. ECS-0335765. The photonic crystal fabrication was supported as part of the Solid-State Solar-Thermal Energy Conversion Center (S3TEC), an Energy Frontier Research Center funded by the U.S. Department of Energy (DOE), Office of Science, Basic Energy Sciences (BES), under Award No. DE-SC0001299/DE-FG02-09ER46577. This work was additionally supported by the Army Research Office through the Institute for Soldier Nanotechnologies under Contract No. W911NF-13-D-0001 and the Micro Autonomous Systems and Technology Collaborative Technology Alliance under Contract No. 892730.

References

- 1 E. Doyle, K. Shukla and C. Metcalfe, *Development and Demonstration of a 25 Watt Thermophotovoltaic Power Source for a Hybrid Power System*, National Aeronautics and Space Administration Technical Report TR04-2001, 2001.
- 2 W. R. Chan, P. Bermel, R. C. N. Pilawa-Podgurski, C. H. Marton, K. F. Jensen, J. J. Senkevich, J. D. Joannopoulos, M. Soljacic and I. Celanovic, *Proc. Natl. Acad. Sci. U. S. A.*, 2013, **110**, 5309–5314.
- 3 C. H. Marton, G. S. Haldeman and K. F. Jensen, *Ind. Eng. Chem. Res.*, 2011, **50**, 8468–8475.
- 4 K. Yoshida, S. Tanaka, S. Tomonari, D. Satoh and M. Esashi, *J. Microelectromech. Syst.*, 2006, **15**, 195–203.
- 5 C.-X. Zu and H. Li, *Energy Environ. Sci.*, 2011, **4**, 2614.
- 6 O. Dessornes, S. Landais, R. Valle, A. Fourmaux, S. Burguburu, C. Zwysig and Z. Kozanecki, *J. Eng. Gas Turbines Power*, 2014, **136**, 071201.
- 7 A. Gomez, J. J. Berry, S. Roychoudhury, B. Coriton and J. Huth, *Proc. Combust. Inst.*, 2007, **31**, 3251–3259.
- 8 A. Kundu, J. H. Jang, J. H. Gil, C. R. Jung, H. R. Lee, S.-H. Kim, B. Ku and Y. S. Oh, *J. Power Sources*, 2007, **170**, 67–78.
- 9 A. Bieberle-Hutter, D. Beckel, A. Infortuna, U. P. Muecke, J. L. M. Rupp, L. J. Gauckler, S. Rey-Mermet, P. Mural, N. R. Bieri, N. Hotz, M. J. Stutz, D. Poulidakos, P. Heeb, P. Müller, A. A. Bernard, R. Gmur, T. Hocker, P. Müller, A. A. Bernard, R. Gmur and T. Hocker, *J. Power Sources*, 2008, **177**, 123–130.
- 10 A. Stambouli and E. Traversa, *Renewable Sustainable Energy Rev.*, 2002, **6**, 433–455.
- 11 W. R. Chan, B. A. Wilhite, J. J. Senkevich, M. Soljacic, J. Joannopoulos and I. Celanovic, *J. Phys.: Conf. Ser.*, 2013, 12017.
- 12 A. Heinzl, V. Boerner, A. Gombert, B. Blasi, V. Wittwer and J. Luther, *J. Mod. Opt.*, 2000, **47**, 2399–2419.
- 13 J. G. Fleming, S. Y. Lin, I. El-Kady, R. Biswas and K. M. Ho, *Nature*, 2002, **417**, 52–55.
- 14 H. Sai, Y. Kanamori and H. Yugami, *Appl. Phys. Lett.*, 2003, **82**, 1685–1687.
- 15 I. Celanovic, N. Jovanovic and J. Kassakian, *Appl. Phys. Lett.*, 2008, **92**, 193101.
- 16 Y. X. Yeng, M. Ghebrebrhan, P. Bermel, W. R. Chan, J. D. Joannopoulos, M. Soljacic and I. Celanovic, *Proc. Natl. Acad. Sci. U. S. A.*, 2012, **109**, 2280–2285.
- 17 C. A. Wang, H. K. Choi, S. L. Ransom, G. W. Charache, L. R. Danielson and D. M. DePoy, *Appl. Phys. Lett.*, 1999, **75**, 1305–1307.
- 18 M. W. Dashiell, J. F. Beausang, H. Ehsani, G. J. Nichols, D. M. Depoy, L. R. Danielson, P. Talamo, K. D. Rahner, E. J. Brown, S. R. Burger, P. M. Fourspring, W. F. Topper, P. F. Baldasaro, C. A. Wang, R. K. Huang, M. K. Connors, G. W. Turner, Z. a. Shellenbarger, G. Taylor, J. Li, R. Martinelli, D. Donetski, S. Anikeev, G. L. Belenky and S. Luryi, *IEEE Trans. Electron Devices*, 2006, **53**, 2879–2888.
- 19 D. Wilt, R. Wehrer, M. Palmisiano, M. Wanlass and C. Murray, *Semicond. Sci. Technol.*, 2003, **18**, S209–S215.
- 20 V. Stelmakh, V. Rinnerbauer, R. D. Geil, P. R. Aimone, J. J. Senkevich, J. D. Joannopoulos, M. Soljačić and I. Celanovic, *Appl. Phys. Lett.*, 2013, **103**, 123903.
- 21 V. Liu and S. Fan, *Comput. Phys. Commun.*, 2012, **183**, 2233–2244.
- 22 E. R. G. Eckert and E. M. Sparrow, *Int. J. Heat Mass Transfer*, 1961, **3**, 42–54.
- 23 W. R. Chan, R. K. Huang, C. A. Wang, J. Kassakian, J. D. Joannopoulos and I. Celanovic, *Sol. Energy Mater. Sol. Cells*, 2010, **94**, 509–514.
- 24 U. Ortabasi, *AIP Conf. Proc.*, 2003, **653**, 249–258.
- 25 P. M. Fourspring, D. M. DePoy, T. D. R. Jr., J. E. Lazo-Wasem and E. J. Gratrix, *Appl. Opt.*, 2006, **45**, 1356–1358.
- 26 O. Ilic, P. Bermel, G. Chen, J. D. Joannopoulos, I. Celanovic and M. Soljačić, *Nat. Nanotechnol.*, 2016, **11**, 1–21.
- 27 Y. X. Yeng, J. B. Chou, V. Rinnerbauer, Y. Shen, S.-G. Kim, J. D. Joannopoulos, M. Soljacic and I. Čelanović, *Opt. Express*, 2014, **22**, 21711.
- 28 M. Zenker and a. Heinzl, *IEEE Trans. Electron Devices*, 2001, **48**, 367–376.
- 29 Y. X. Yeng, W. R. Chan, V. Rinnerbauer, J. D. Joannopoulos and I. Celanovic, *Opt. Express*, 2013, **21**, 2879–2891.
- 30 N. Wang, L. Han, H. He, N.-H. Park and K. Koumoto, *Energy Environ. Sci.*, 2011, **4**, 3676–3679.